Impact of the Ionosphere on an L-band Space Based Radar

Elaine Chapin, Samuel F. Chan, Bruce D. Chapman, Curtis W. Chen, Jan M. Martin,
Thierry R. Michel, Ronald J. Muellerschoen, Xiaoqing Pi, and Paul A. Rosen
Jet Propulsion Laboratory
California Institute of Technology
Pasadena, California 91109-8099
Email: Elaine.Chapin@jpl.nasa.gov

***Abstract*— We have quantified the impact that the ionosphere would have on a L-band interferometric Synthetic Aperture Radar (SAR) mission using a combination of simulation, modeling, Global Positioning System (GPS) data collected during the last solar maximum, and existing spaceborne SAR data.**

Using the Jet Propulsion Laboratory's Global Ionospheric Maps (GIM) total electron content (TEC) estimates derived from the worldwide array of GPS stations, we determined that the sun synchronous orbit which would minimize TEC at the time of imaging has dawn and dusk equator crossings. Such an orbit also avoids the equatorial post-sunset irregularities. We used the GIM data to examine the day-to-day variability in the background ionosphere and to quantify the impact of the background ionosphere on single pass SAR performance. With the exception of Faraday rotation related effects on single polarization systems, degradation due to the background ionosphere can be avoided if a reasonable model for the ionosphere is used during processing. Our studies reveal that Faraday rotation angles rarely exceeded the 10° threshold that impacts biomass retrieval and that repeat pass interferometric SAR decorrelation due to variations in the background ionosphere causing variable Faraday rotations is a negligible effect.

Even a dawn-dusk orbit will not avoid high latitude ionospheric irregularities. We evaluated the strength of the ionospheric irregularities using GPS scintillation data collected at Fairbanks, Alaska and modeled the impact of these irregularities on azimuth resolution, azimuth displacement, peak sidelobe ratio (PSLR), and integrated sidelobe ratio (ISLR). Our examination of ionospheric artifacts in InSAR data has revealed that the artifacts occur primarily in the polar cap data, not auroral zone data as was previously thought.

I. Introduction

L-band spaceborne SARs provide critical earth science measurements. Solid earth studies of seismic and volcanic deformation benefit from the low temporal decorrelation of L-band data, a critical performance element for repeat pass interferometric SAR (InSAR). L-band's demonstrated ability to penetrate into dry sand and vegetation makes it a valuable tool for diverse fields such as archaeology and biomass retrieval. However, radar performance degradation due to the ionosphere remains a concern for L-band and lower frequency spaceborne radars, despite the success of previous L-band spaceborne SARs such as SeaSAT, the JERS-1 SAR, and the Shuttle Imaging Radar (SIR-A/B/C). (See, for example, the recent comprehensive review by Xu et al. [1] and the references therein.) Here we examine several of those concerns and conclude that, except at high latitudes, the ionosphere will not significantly impact the performance of an L-band InSAR mission.

II. Orbit Selection

An ideal orbit would minimize the background ionosphere total electron content for both the ascending and descending passes, minimize the day to day variance of the background ionosphere total electron content for both the ascending and descending passes, and minimize the probability of encountering ionospheric irregularities. We considered only sun synchronous orbits with a 506 km altitude at the equator, 0.001279 eccentricity, 90° argument of periapse, 5 day ground track repeat, and 97.4° inclination. The local times (LT) of the ascending nodes for the tested cases were 4:00 a.m., 5:00 a.m., 6:00 a.m., 7:00 a.m., and 8:00 a.m.

We excluded from consideration orbits with ascending equatorial crossings from 0:00 - 3:00 LT since the descending passes would pass through the peak of the daily ionization. The most severe irregularities occur at low latitudes, near the earth's magnetic equator. Equatorial scintillation occurs almost exclusively in the post-sunset period sometimes extending until dawn [2] [3]. To avoid equatorial irregularities on the descending arcs, orbits with equatorial crossing times from 9:00 to 12:00 LT were excluded.

Both this orbit selection study and the background ionosphere Faraday rotation study used the global TEC maps inferred from GPS data. The JPL GPS-based global ionospheric maps (GIM) use dual-frequency (L-band) GPS measurements from over 100 ground receiver locations to produce a global map of vertical ionospheric total electron content (TEC). There is an abundance of stations in Europe and the continental US and a sparsity of stations in Africa, in the oceans, and at high latitudes. The quality of the GIM TEC is poorer the farther the geographic location is from a station. The GIM provides a measure of integrated column density up to GPS altitudes (20,200 km). For this study we used year 2000 data, near the last solar max. GIM global estimates of TEC are provided every 15 minutes.

Because the low earth orbits considered are significantly below the GPS satellites' altitude, the fraction of the ionospheric TEC above the spacecraft needs to be excluded. Roughly half

of the ionospheric electrons are above 500 km. The fraction of the TEC to exclude is calculated using the International Reference Ionosphere (IRI). At each time and location for which a GIM TEC was extracted, the IRI model was run producing a vertical electron density profile. The fraction of the TEC below the spacecraft was calculated from the profile, and the GIM estimate the TEC was correspondingly reduced.

Figure 1 shows the mean scaled TEC for the ascending arcs which image the low and mid-latitudes near dawn. Figure 2 shows the mean scaled TEC for the descending arcs which image the low and mid-latitudes near dusk. These figures were accumulated by simulating the flying of the spacecraft in a given orbit for a year. Using the GIM data and the IRI model, the TEC below the spacecraft was extracted each time the spacecraft entered a new 1° cell.

Comparing the TEC plots for different orbits in Figure 1, the dominant feature is the increase in the TEC for the orbits imaging the earth later in the morning. Similarly the dominant feature in Figure 2 is the decrease in the TEC of the orbits imaging the earth later in the evening. The enhancements of ionization above and below the magnetic equator, known as the equatorial anomaly, are clearly visible in the evening data.

Table I shows the summary statistics for the five candidate orbits considered. For each orbit arc, the average world grid of mean TECs and the average standard deviation of the world grid of mean TECs is listed. In general, the higher the average scaled TEC, the higher the average standard deviation. The standard deviation reflects the day to day variability in the background ionosphere at a given location and time of day.

If the goal was to select an orbit that minimized the TEC on one arc, the best choice orbit would be the 4:00 a.m. equatorial crossing since its ascending arc has the lowest average mean TEC of 8.01 TECU. The best compromise choice with reasonable TEC for both arcs and the lowest overall TEC is the 6:00 a.m. equatorial crossing orbit with an average of 18.73 TECU.

Orbit Time of Ascending Node	Arcs	Time of Equator Crossing [LT]	Average TEC [TECU]	Average Standard Deviation
4 AM	asc	4 AM	8.01	3.88
5 AM	asc	5 AM	8.04	4.28
6 AM	asc	6 AM	10.41	5.40
7 AM	asc	7 AM	15.91	6.30
8 AM	asc	8 AM	22.12	6.90
4 AM	desc	4 PM	33.72	9.42
5 AM	desc	5 PM	30.87	9.00
6 AM	desc	6 PM	27.06	8.65
7 AM	desc	7 PM	22.64	8.10
8 AM	desc	8 PM	19.30	7.60
4 AM	both	4 AM + PM	20.86	
5 AM	both	5 AM + PM	19.46	
6 AM	both	6 AM + PM	18.73	
7 AM	both	7 AM + PM	19.27	
8 AM	both	8 AM + PM	20.71	

TABLE I

SUMMARY TABLE COMPARING TEC FOR VARIOUS CANDIDATE ORBITS.

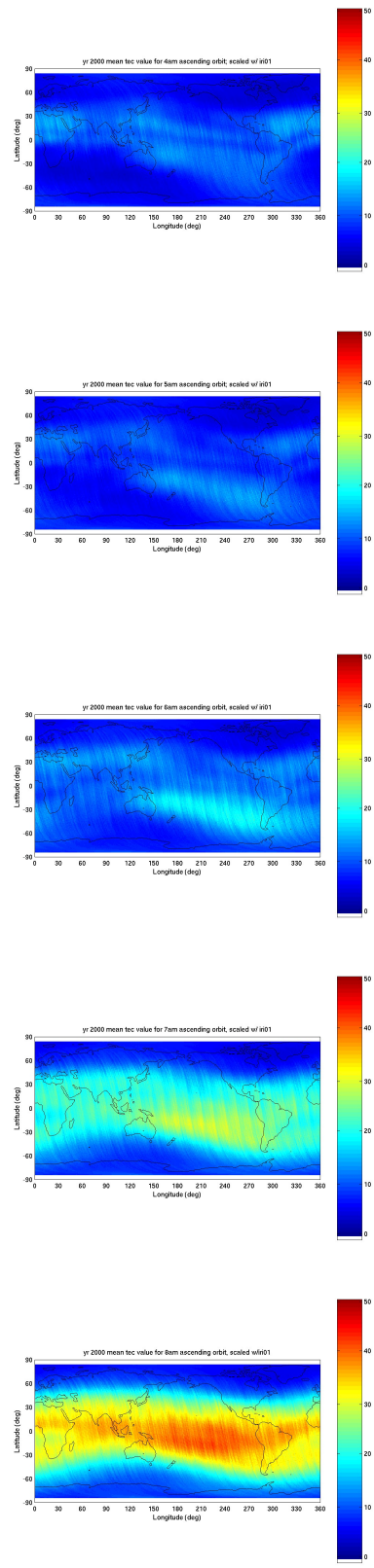

Fig. 1. Mean scaled TEC value for the ascending arcs for the orbits with equatorial crossings at 4:00 a.m., 5:00 a.m., 6:00 a.m., 7:00 a.m., and 8:00 a.m.. Color indicates scaled TEC with dark red indicating 50 TECU.

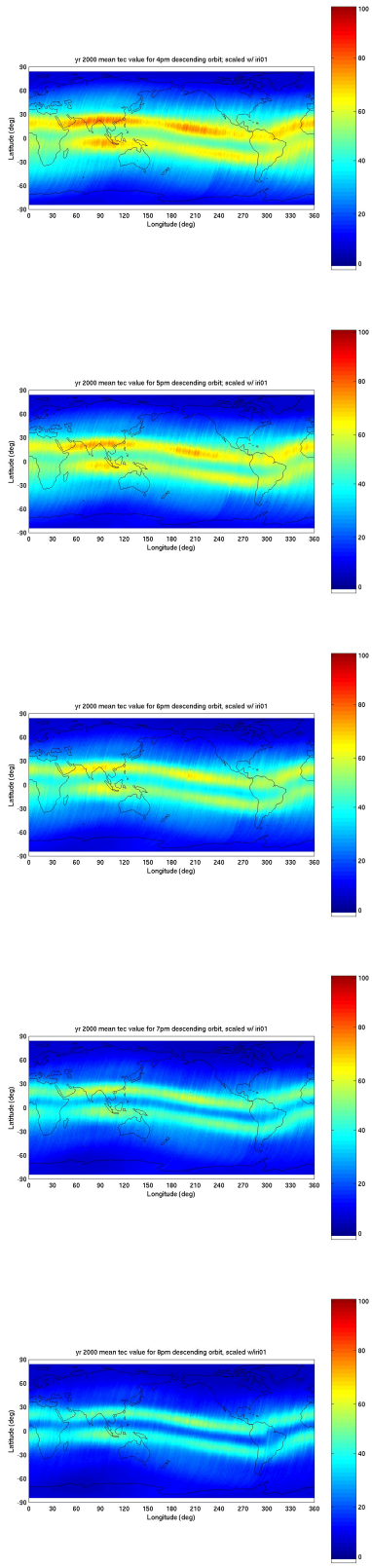

Fig. 2. Mean scaled TEC value for the descending arcs for the orbits with equatorial crossings at 4:00 a.m., 5:00 a.m., 6:00 a.m., 7:00 a.m., and 8:00 a.m.. Color indicates scaled TEC with dark red indicating 100 TECU.

III. Impact of Faraday Rotation

Given concerns that the ionosphere would corrupt targets' polarimetric signatures [4] [5] and cause interferometric decorrelation, we have examined the impact of a realistic, variable, background ionosphere on a single pass and repeat pass interferometric L-band SAR flying in a realistic orbit. The purpose of the simulation is to establish the magnitude of the errors introduced by the background ionosphere on InSAR measurements. Results are reported for a right looking 80 MHz bandwidth repeat-pass L-band InSAR with a 50 m long antenna viewing a 200 km wide swath with a 45° near range look angle and a 2° squint angle flying in a sun-synchronous orbit.

The dispersion relation of radio waves in a magnetized plasma was used to compute the point spread function (PSF) of focused SAR data acquired in the presence of a temporally and spatially dependent background ionosphere derived from Global Positioning System (GPS) data. The formulation assumes that the radar signal propagates along paths described by the laws of geometrical optics in free-space. The ionosphere affects this free-space propagation through a frequency, polarization, and path dependent phase delay. The path-dependence of the phase delays is obtained by using a thin shell model for the ionosphere. Other ionosphere scattering effects such as diffraction, refraction, and interference of waves within the antenna aperture are not taken into account. Defocusing effects within the synthetic aperture are considered to first order. The resulting PSF contains ionospheric effects such as azimuth and range displacements, pulse broadening, defocusing, and Faraday rotation. The simulation consists of computing, analyzing, and collecting the PSFs of the focused SAR data for ionospheric conditions sampled at five sites twice a day for two years. All simulation parameters except the ionospheric conditions are kept constant throughout the time series.

The background ionosphere data used in the study are GPS-derived TEC maps updated every 15' (GIM). The width of the smallest features observed in the horizontal distribution of TEC is about 500 km. The vertical structure of the ionosphere was modeled using the International Reference Ionosphere (IRI), and the International Geomagnetic Reference Field (IGRF) was used to model the Earth's magnetic field.

Five study sites were considered: Arequipa, Peru; Bogota, Colombia; Santiago, Chile; North Liberty, Iowa; and Fairbanks, Alaska. These sites were selected because their geographic distribution represents different types of phenomena expected with varying geomagnetic latitude and because they are co-located with some of the GPS receivers used by the GIM. Approximate times-of-day for imaging during the ascending and descending passes for these locations are given in Table II. These times are computed using the sun-synchronous orbit described previously which intersects the equator at local times near 06:00 (ascending) and 18:00 (descending).

Single pass point target response degradations were evaluated and shown to be small. The PSF broadening and PSLR/ISLR reduction, are less than 10% of their unperturbed

Site	Latitude [deg]	Longitude [deg]	LST dawn pass	LST dusk pass
Arequipa	-16.46	288.50	6:09:00	17:54:00
Bogota	4.64	285.92	5:57:36	18:00:00
Santiago	-33.15	289.33	6:19:48	17.42:00
North Liberty	41.77	268.42	5:33:36	18:24:00
Fairbanks	64.98	212.50	4:54:36	19:06:00

TABLE II

POSITIONS AND LOCAL SOLAR TIME (LST, HH:MM:SS) FOR THE DAWN (ASCENDING) AND DUSK (DESCENDING) PASSES.

values if the processing ignores the ionospheric medium. If a realistic model for the TEC were used in the SAR processing, much of the point target response degradation would be removed.

Figure 3 shows the variation in TEC below the spacecraft's orbit at the dusk imaging time at Santiago over a 2 year interval overlapping the 2000 solar maximum. There is considerable daily and seasonal variation of the ionospheric TEC. The TEC maxima occur near the equinoxes and minima occur around the summer and winter solstices, although the minimum is deeper during austral winter. For each site, the dawn imaging time has both a lower TEC and lower TEC variability than the dusk imaging time. Figure 3 shows the TEC derived only from the IRI and the scaled GIM TEC measurement. The mean and root mean square (RMS) TEC differences between the two TEC time series are 3.9 TECU and 10.7 TECU, respectively. The day to day variations as well as the seasonal variations are significantly larger in the GIM data than in the IRI model.

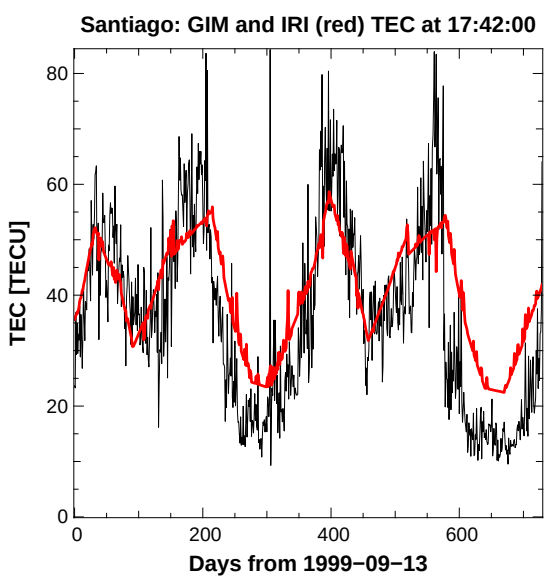

Fig. 3. The GIM (black) and IRI (red) data for the height-adjusted TEC above Santiago for a two year period starting on the 13 September 1999 sampled daily at the time of the dusk pass (17:42:00 local solar time).

Table III summarizes the key ionospheric parameters derived from the GIM, the IRI, and the IGRF for the two years studied for the five sites and the two imaging times. The TEC for all sites and passes was always below 100 TECU. At the equator for the evening imaging time, the TEC was typically 50 TECU. The primary variation in the TEC is the seasonal trend, which is captured in the standard models such as the IRI. The ionospheric TEC generally decreases, and the magnetic field strength generally increases toward the poles. The magnetic angle is the angle between the look vector from the radar to the target and the geomagnetic field vector, $\vec{\mathbf{B}}_E$. Near the magnetic equator, the imaging is approximately perpendicular to the magnetic field while at high latitudes the imaging direction is better aligned with the magnetic field lines.

Site and Pass	Scaled TEC [TECU]	Magnetic Angle [deg]	$\lVert \vec{\mathbf{B}}_E \rVert$ [gauss]	Ionospheric Height [km]
Arequipa AM	15.1 ± 8.1	110.3 ± 0.1	0.20	322.9 ± 8.9
Arequipa PM	38.6 ± 10.9	109.8 ± 0.1	0.20	394.7 ± 8.1
Bogota AM	12.3 ± 4.0	85.1 ± 0.1	0.25	331.7 ± 5.6
Bogota PM	52.8 ± 15.2	84.7 ± 0.2	0.25	361.3 ± 1.2
Santiago AM	17.9 ± 10.9	122.0 ± 0.1	0.20	332.0 ± 7.6
Santiago PM	36.4 ± 16.7	122.0 ± 0.1	0.20	338.9 ± 10.6
North Liberty AM	7.0 ± 3.4	55.8 ± 0.3	0.43	346.6 ± 19.1
North Liberty PM	18.7 ± 5.8	55.8 ± 0.1	0.43	346.5 ± 7.2
Fairbanks AM	6.0 ± 3.2	46.9 ± 0.3	0.45	366.5 ± 22.8
Fairbanks PM	7.1 ± 3.4	47.1 ± 0.1	0.45	353.2 ± 11.2

TABLE III

AVERAGES AND RMS VARIATIONS OF SOME IONOSPHERE PROPERTIES OVER THE TWO YEAR PERIOD FOR THE DAWN (AM) AND DUSK (PM) IMAGING TIMES.

The dependence of the background TEC on time of day, latitude, and time of year also applies to the distribution of Faraday rotation angles observed. However another important factor in the geographic sensitivity of the Faraday rotation comes from the magnitude and orientation of the Earth magnetic field $\vec{\mathbf{B}}_E$. Of the sites and passes considered, the largest Faraday rotation angles were seen in the dusk pass at Santiago, shown in Figure 4, and the dusk pass at North Liberty. Table IV lists the average Faraday rotation angle for each site and pass.

Two-way rotations exceeding 10° may impact geophysical parameter recovery [4]. As shown in Table IV, this 10° threshold is rarely exceeded for our orbit. The morning data collections are always below the threshold. The threshold is exceeded in the evening data near the geographic equator where the TEC values are large and at the higher latitudes where the magnetic field strength is larger. Although Faraday rotation can cause a reduction in the signal to noise ratio of a single polarization radar, this will not be a significant effect given the size of the Faraday rotations observed.

We evaluated realistic target displacements if the data processing were done assuming vacuum between the radar and the ground. This displacement is primarily in range and could be compensated for, almost entirely, by using GIM or the equivalent data during processing. The displacements of the point of maximum power in the PSF from their true target positions are larger in range than in azimuth, as seen in

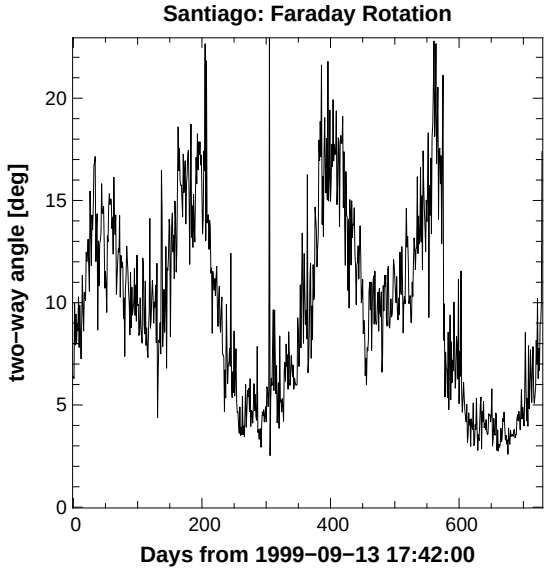

Fig. 4. The two-way Faraday rotation angle in degrees for a two year period starting on the 13 September 1999 sampled daily at the time of the dusk pass above Santiago (17:42:00 local solar time).

Site and Time	Two Way Faraday Rotation Angle [deg]	Range Displacement [m]	Azimuth Displacement [m]
Arequipa AM	2.6 ± 1.4	5.6 ± 3.0	0.6 ± 0.3
Arequipa PM	6.4 ± 1.8	14.3 ± 4.0	1.9 ± 1.6
Bogota AM	0.7 ± 0.2	4.5 ± 1.5	1.0 ± 0.4
Bogota PM	3.0 ± 0.9	19.5 ± 5.6	0.4 ± 1.4
Santiago AM	4.9 ± 3.0	6.6 ± 4.0	0.6 ± 0.4
Santiago PM	9.9 ± 4.5	13.4 ± 6.2	3.2 ± 1.3
N. Liberty AM	4.3 ± 2.0	2.6 ± 1.2	0.0 ± 0.2
N. Liberty PM	11.3 ± 3.5	6.9 ± 2.1	0.6 ± 0.6
Fairbanks AM	4.6 ± 2.5	2.2 ± 1.2	0.2 ± 0.3
Fairbanks PM	5.4 ± 2.6	2.6 ± 1.3	0.4 ± 0.3

TABLE IV

AVERAGES AND RMS VARIATIONS OF BACKGROUND IONOSPHERIC EFFECTS OVER THE TWO YEAR PERIOD.

Table IV. Range displacements are caused by the slope (group velocity) of the dispersion relation at the center frequency and they are proportional to the TEC. Azimuth displacements have two different physical origins. First, the squint angle transforms a small fraction of the range displacement into an along track displacement. A larger contribution to the azimuth displacement is due to small slopes in the GIM TEC in the along track direction. A TEC gradient creates a phase ramp across the synthetic aperture which, in turn, manifests itself as an azimuth displacement. The largest azimuth displacements are 6 m, about a quarter of the azimuth resolution. Range displacement can be as large as 36 m, 20 times larger than the range resolution.

Our simulation results show that Faraday rotation induced InSAR decorrelations are much less than 1% for the sun synchronous orbit considered. Table V gives the summary decorrelation statistics for all sites, both imaging times, HH and VV polarization InSARs, and two choices for the range of scattering matrices considered. The Faraday rotation induced interferometric decorrelation was estimated in the following manner. The one-dimensional time series for the two-way rotation angles (as shown for example in Figure 4) were used to compute a two-dimensional time-lag array of Faraday decorrelations. Statistics were computed for the decorrelation values considering one-way lags (each pair counted only once) and after eliminating lags with too few realizations (< 365). Because the amount of interferometric decorrelation for a given Faraday rotation angle depends on the scattering matrix, we allowed the scattering matrices to vary within a range such that they maximized the decorrelation. We used two ranges, one corresponding to realistic targets and another unphysical range designed determine the worst case decorrelation. Because the Faraday rotation angle difference between passes is small, less than 10° as shown in the variances in Table IV, the decorrelation caused by the Faraday rotation angle difference is small.

Polarization: Scattering:	VV Realistic	VV Unphysical	HH Realistic	HH Unphysical
Arequipa AM	$1.5\ 10^{-6}$	$1.2\ 10^{-5}$	$1.6\ 10^{-7}$	$2.5\ 10^{-6}$
Arequipa PM	$7.0\ 10^{-6}$	$5.3\ 10^{-5}$	$7.8\ 10^{-7}$	$1.1\ 10^{-5}$
Bogota AM	$1.4\ 10^{-9}$	$1.6\ 10^{-8}$	$1.7\ 10^{-10}$	$3.3\ 10^{-9}$
Bogota PM	$4.3\ 10^{-7}$	$3.6\ 10^{-6}$	$4.7\ 10^{-8}$	$7.2\ 10^{-7}$
Santiago AM	$1.8\ 10^{-5}$	$1.4\ 10^{-4}$	$2.0\ 10^{-6}$	$2.9\ 10^{-5}$
Santiago PM	$1.6\ 10^{-4}$	$1.2\ 10^{-3}$	$1.8\ 10^{-5}$	$2.5\ 10^{-4}$
North Liberty AM	$5.6\ 10^{-6}$	$4.7\ 10^{-5}$	$6.4\ 10^{-7}$	$9.5\ 10^{-6}$
North Liberty PM	$1.4\ 10^{-4}$	$9.9\ 10^{-4}$	$1.5\ 10^{-5}$	$2.0\ 10^{-4}$
Fairbanks AM	$1.2\ 10^{-5}$	$8.8\ 10^{-5}$	$1.3\ 10^{-6}$	$1.7\ 10^{-5}$
Fairbanks PM	$1.3\ 10^{-5}$	$1.0\ 10^{-4}$	$1.4\ 10^{-6}$	$2.0\ 10^{-5}$

TABLE V

SUMMARY OF THE MAXIMUM 90% INSAR DECORRELATION VALUE OVER A ONE YEAR MAXIMUM TIME LAG.

Because the ionospheric TEC has a strong seasonal dependence, the decorrelation varies strongly with the temporal separation between the two passes. In general, the highest decorrelations are for lags of 3 months and 9 months with smaller decorrelations for 6 months and 12 months.

Processing single pass L-band SAR data as if there is vacuum between the radar and the ground results in a phase ramp across the swath, the size of which is largely determined by the TEC. This ramp can be up to 200 rad. These ramps are due to look angle diversity across the swath. If an interferogram is formed using two passes of data, each of which have different ramps because of different ionospheric conditions at the imaging times, the interferogram will also have a phase ramp which could complicate unwrapping and confuse ionospheric and geophysical signals. The effect could be largely eliminated by using GIM or the equivalent data when processing the single pass data.

IV. IMPACT OF AURORAL ZONE SCINTILLATION

Although the orbit can be selected to avoid the post-sunset equatorial ionospheric scintillation, auroral zone and polar cap

ionospheric irregularities may still create artifacts in L-band spaceborne SAR data. We investigated the impact auroral zone scintillation would have on SAR performance using GPS L1 phase scintillation measurements [6] collected at Fairbanks, Alaska, during the peak of solar activity of the last solar cycle, the year 2000. For this work, we assumed that the ionospheric irregularities were 350 km above the surface in a layer 50 km thick, that the anisotropic irregularity axis ratio was 5, that the irregularities obeyed a two-slope spectrum with inner and outer spectral indices of 1.5 and 2.5, that the inner scale and break scale were 100 m and 500 m, that the outer scale for the GPS phase scintillation measurements was 10 km, and that the outer scale for the radar measurements was 30 km. We developed a method of estimating the strength of the irregularity spectrum from each GPS phase scintillation measurement [7] using these assumptions and using a phase screen model with an anisotropic irregularity spectrum with irregularities elongated along the geomagnetic field lines [8]. We then used each spectrum to calculate the impact on radar performance for an L-band radar on a spacecraft 506 km above the surface with a 10 m long antenna viewing targets at a look angle of 35°. The impact of ionospheric scintillation on the azimuth resolution, range resolution, and pulse broadening was calculated based on a published model [9] [10] while a model following Tartarski [11] was used to estimate the effects on radar image azimuth displacement. The thousands of estimates of radar performance degradation were accumulated to produce statistical measures of the impact of scintillation.

Figure 5 shows summary histograms of the frequency of occurrence of various levels of ionospheric degradation. The histograms were built using all of the available GPS scintillation data without sorting the data in time or by geomagnetic activity level. An azimuth resolution degradation of 10% indicates that the resolution was 10% worse than the azimuth resolution expected in the presence of no ionosphere. Similarly, an azimuth displacement degradation of 10% indicates that a target would be displaced by one tenth of an azimuth resolution element. It is clear from the figure that only a small percentage, less than 5%, of the data shows any significant degradation in performance. The probability of azimuth resolution degradation by more than 2% of the ideal value is less than 4%. The likelihood of PSLR or ISLR degradation larger than 2 dB is less than 3%. The probability of azimuth displacements larger than 10% is less than 5%.

Auroral zone scintillation has a well known dependence on time of day, time of year, and geomagnetic activity – an effect that is averaged over in Figure 5. In particular, scintillation is more common at night, especially in the midnight to dawn sector near the equinoxes. Figure 6 shows how frequently the azimuth displacement is one tenth of an azimuth pixel or greater as a function of local time of day and month. Because auroral zone sites imaged in the pre-dawn hours have a non-negligible probability of being corrupted with ionospheric irregularity artifacts, careful planning of data acquisitions with respect to season and ascending vs. descending pass is recommended. For any sun-synchronous orbit, scintillation

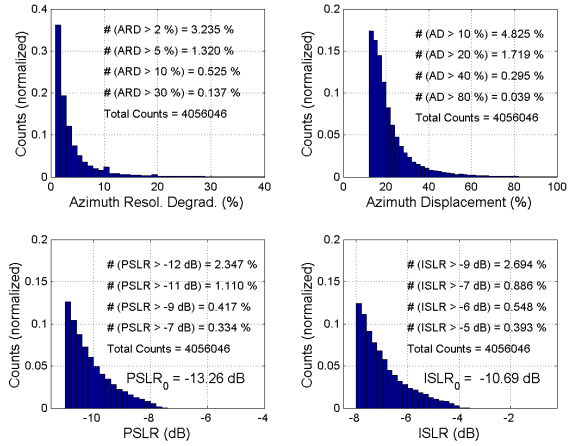

Fig. 5. Normalized histograms showing the frequency of occurrence of degradations in radar performance due to ionospheric scintillation. Only the tails are plotted for clarity. The system resolution, PSLR, and ISLR if no ionosphere were present are 5 m, -13.26 dB, and -10.69 dB.

will be more probable for some auroral zone longitudes than others because the local time of imaging will vary due to the offset between geographic and geomagnetic latitude.

The ionospheric irregularities at auroral latitudes are closely correlated to space weather conditions that enhance the auroral electrojet causing magnetic field perturbations in the ionosphere and on the ground. These magnetic field perturbations can be an indicator of the effects on possible degradation of radar images. There is a clear correlation between the degradation of space based radar performance in the auroral zone passes and auroral electrojet activity characterized by the AE index [12]. The latter significantly increases with disturbed space weather conditions. Figure 7 shows the mean degradation of radar azimuth resolution vs. the auroral electrojet index (AE). To obtain the plot, the estimated azimuth resolution degradation (R) was binned at 50 γ intervals and then averaged. As AE increases to the 1000 γ level, the average degradation of azimuth resolution can be larger than 2%. A quadratic fit is also included in the plot. It is clear that the AE index could be used to predict which auroral zone SAR scenes might be corrupted by ionospheric irregularities.

V. Azimuth Shifts

Repeat pass SAR interferometry is affected by the ionosphere. Changes in background ionosphere between passes lead to phase ramps which are generally absorbed by the baseline estimation procedure. Of more concern are ionospheric irregularities which produce high frequency (kilometer horizontal scale) bands of azimuth mis-registration (up to half a pixel) and ripples in the interferometric phase [13] [14]. Glaciologists have observed these “azimuth streaks” in the much of the high latitude data from the ERS-1, ERS-2, RADARSAT-1, JERS-1, and ENVISAT satellites. If irregularities are present on either of the two collections used for an interferometric pair, the data can be corrupted.

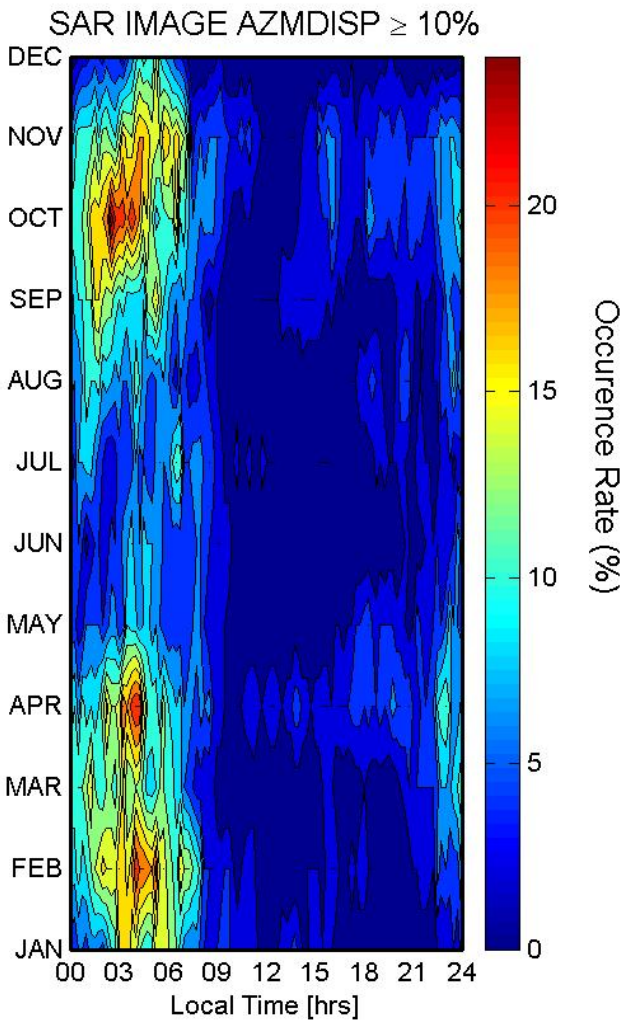

Fig. 6. Frequency of occurrence that the azimuth displacement due to ionospheric scintillation exceeds 10% (a tenth of an azimuth resolution element which is 50 cm) plotted as a function of time of year and local time.

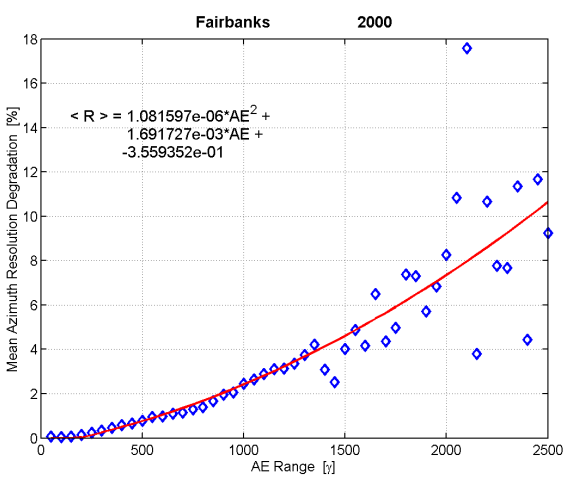

Fig. 7. Mean degradation of the azimuth resolution due to ionospheric scintillation versus the auroral electrojet activity as characterized by the AE index.

A preliminary evaluation of already processed in-house InSAR data imaging both Antarctica and Greenland revealed that azimuth streaks occur much more frequently in polar cap data than for sites in the auroral zone. This conclusion that azimuth streaks are essentially a polar cap phenomenon is supported by observations scintillation caused by kilometer scale irregularities in the polar cap [15] and is consistent with the auroral zone analysis of the previous section which showed that auroral zone azimuth displacements are too infrequent to account for the fraction of InSAR data effected.

We obtained RADARSAT-1 data covering two two polar cap sites, Petermann Gletscher in Northern Greenland (Petermann) and a site in coastal Antarctica near McMurdo (McMurdo). We processed 15 passes making 11 offset fields at Petermann and 5 passes making 7 offset fields at McMurdo. 87% (13/15) of the Petermann pairs and all of the McMurdo pairs exhibited streaks. For each interferometric pair where streaks were present, we evaluated the density of streaks per kilometer of spacecraft travel along track, the width of the streaks, the maximum azimuth shift, and the orientation of the streaks. Each site showed a consistent orientation of the azimuth streaks which may be related to the angle between the look vector and the magnetic field. However, with only two sites it is difficult to make firm conclusions on this point.

We found no correlation between the presence of azimuth streaks or the severity of azimuth streaks with ionospheric indices such as Kp or the polar cap index, the orientation of the interplanetary magnetic field (IMF), the convection maps measured by the SuperDARN network, or fluctuations in the magnetometer data collected at Qanaaq located near the Petermann site. The lack of correlation with ionospheric measurements is surprising given the known qualitative differences in polar cap ionospheric phenomena (patches, blobs, sun-aligned arcs, etc.) as a function of the IMF driven convection [16] [17].

There was a correlation with season and TEC. Streaks were less frequent during local winter. For the two Petermann offset fields with no streaks, all four passes were collected in the local winter when the TEC extracted from the GIM data was very low (< 4 TECU). This correlation is surprising given the pronounced minimum in measured polar cap scintillation during local summer [18] [19]. The scintillation causing the azimuth streaks may be associated with the relative scintillation maximum observed during summer months near magnetic noon [20]. The seasonal dependence implies that azimuth streaks are not associated with polar cap patches [21]. The seasonal dependence may also explain the lack of correlation of the frequency of occurrence with ionospheric measurements because convection is less important in the summer hemisphere when convecting structures decay more rapidly [22].

VI. Conclusions and Future Work

We have determined that a dawn-dusk sun-synchronous orbit minimizes the ambient ionospheric density below the spacecraft. The data produced by an L-band InSAR in such

an orbit will not be corrupted by significant artifacts due to the presence of the variable background ionosphere. Most of the artifacts, such as the small degradation in the point target response, could be removed by using a background ionosphere model during processing. Evaluating the required model accuracy and developing processing techniques which apply the model would be valuable next steps.

Our analysis indicates that auroral zone scintillation which could impact SAR performance occurs less than 5% of the time. However, the frequency of occurrence of scintillation will vary for different locations in the auroral zone because they will be imaged at different local times because of the mis-alignment of geographic and geomagnetic latitude. The probability of degradation is strongly correlated with ionospheric activity as characterized by the ionospheric indices and has a distinct time of day and time of year dependence. Appropriate acquisition planning of auroral zone collections is recommended. An analysis of artifacts in JERS-1 and PALSAR auroral data to verify our conclusions would be valuable.

Additional work characterizing polar cap scintillation and the observed azimuth shifts is needed. Azimuth shifts are more commonly observed in the polar cap than in the auroral zone and are least frequent during local winter. We observed no correlation between the occurrence of streaks with the ionospheric Kp or PC indices or northward or southward IMF. Given the prevalence of azimuth shifts in the existing polar cap C-band SAR data, development of a scheme to compensate for the shifts would be valuable.

Acknowledgment

The authors would like to thank Brian Wilson for contributing the GIM database for our analysis. The authors would like to thank Eric Rignot, Ron Kwok, and Ian Joughin for providing data and useful discussions regarding azimuth streaks. This work was performed at the Jet Propulsion Laboratory, California Institute of Technology under a contract with the National Aeronautics and Space Administration.

References

[1] Z.-W. Xu, J. Wu, and Z.-S. Wu, "A survey of ionospheric effects on space-based radar," *Waves in Random Media*, vol. 14, no. 2, pp. S189–S273, April 2004. [Online]. Available: http://www.iop.org/EJ/abstract/0959-7174/14/2/008

[2] S. Basu, E. M. MacKenzie, and S. Basu, "Ionospheric constraints on VHF/UHF communication links during solar maximum and minimum periods," *Radio Sci.*, vol. 23, no. 3, pp. 363–378, 1988.

[3] S. Basu, K. M. Groves, S. Basu, and P. J. Sultan, "Specification and forecasting of scintillations in communication/navigation links: Current status and future plans," *Journal of Atmospheric and Solar-Terrestrial Physics*, vol. 64, no. 16, pp. 1745–1754, 2002.

[4] P. A. Wright, S. Quegan, N. S. Wheadon, and C. D. Hall, "Faraday rotation effects on L-band spaceborne SAR data," *IEEE Trans. Geosci. Remote Sensing*, vol. 41, no. 12, pp. 2735–2744, December 2003.

[5] A. Freeman and S. S. Saatchi, "On the detection of Faraday rotation in linearly polarized L-band SAR backscatter signatures," *IEEE Trans. Geosci. Remote Sensing*, vol. 42, no. 8, pp. 1607–1616, August 2004.

[6] X. Pi, S. Nandi, D. A. Stowers, M. R. Marcin, U. J. Lindqwister, M. J. Reyes, A. W. Moore, D. N. Fort, and J. A. Klobuchar, "Development of ionospheric scintillation monitoring system using receivers of the igs global gps network," in *Proceedings of the 55th Annual ION Meeting*, Cambridge, Massachusetts, June 1999, pp. 395–402.

[7] X. Pi and S. F. Chan, "Analysis of ionospheric scintillation effects on space-based radar systems," Tech. Report, Jet Propulsion Laboratory, Pasadena, CA, Tech. Rep., September 2005.

[8] C. L. Rino, "A power law phase screen model for ionospheric scintillation 1. Weak scatter," *Radio Sci.*, vol. 14, no. 6, pp. 1135–1145, 1979.

[9] A. Ishimaru, Y. Kuga, J. Liu, Y. Kim, and T. Freeman, "Ionospheric effects on synthetic aperture radar at 100 MHz to 2 GHz," *Radio Sci.*, vol. 34, no. 1, pp. 257–268, 1999.

[10] J. Liu, Y. Kuga, A. Ishimaru, X. Pi, and A. Freeman, "Ionospheric effects on SAR imaging: a numerical study," *IEEE Trans. Geosci. Remote Sensing*, vol. 41, no. 5, pp. 939–947, May 2003.

[11] V. I. Tatarski, *The Effects of the Turbulent Atmosphere on Wave Propagation.* Jerusalem: Isreal Program for Scientific Translations, 1971.

[12] P. N. Mayaud, *Derivation, Meaning and Use of Geomagnetic Indices.* Washington D.C.: Am. Geophys. Union, 1980.

[13] I. Joughin, D. Winebrenner, M. Fahnestock, R. Kwok, and W. Krabill, "Measurement of ice-sheet topography using satellite-radar interferometry," *Journal of Glaciology*, vol. 42, no. 140, pp. 10–22, 1996.

[14] A. L. Gray, K. E. Mattar, and G. Sofko, "Influence of ionospheric electron density fluctuations on satellite radar interferometry," *Geophysical Research Letters*, vol. 27, no. 10, pp. 1451–1454, 2000.

[15] J. W. MacDougall, "Distribution of irregularities in the northern polar region determined from HILAT observations," *Radio Sci.*, vol. 25, no. 2, pp. 115–124, 1990. [Online]. Available: http://www.agu.org/pubs/crossref/1990/89RS03328.shtml

[16] H. C. Carlson, Jr., "The dark polar ionosphere: Progress and future challenges," *Radio Sci.*, vol. 29, no. 1, pp. 157–165, 1994. [Online]. Available: http://www.agu.org/journals/rs/rs9401/93RS02125.pdf

[17] S. Basu and C. Valladares, "Global aspects of plasma structures," *Journal of Atmospheric and Solar-Terrestrial Physics*, vol. 61, no. 1, pp. 127–139, 1999.

[18] S. Basu, S. Basu, E. MacKenzie, and H. E. Whitney, "Morphology of phase and intensity scintillations in the auroral oval and polar cap," *Radio Sci.*, vol. 20, no. 3, pp. 347–356, 1985.

[19] S. Basu, E. M. MacKenzie, S. Basu, E. Costa, P. F. Fougere, H. C. Carlson, Jr., and H. E. Whitney, "250 MHz/GHz scintillation parameters in the equatorial, polar, and auroral environment," *IEEE Journal on Selected Areas in Communication*, vol. 5, no. 2, pp. 102–115, February 1987.

[20] L. Kersley, C. D. Russell, and D. L. Rice, "Phase scintillation and irregularities in the northern polar ionosphere," *Radio Sci.*, vol. 30, no. 3, pp. 619–629, 1995.

[21] S. Basu, S. Basu, J. J. Sojka, R. W. Schunk, and E. MacKenzie, "Macroscale modeling and mesoscale observations of plasma density structures in the polar cap," *Geophysical Research Letters*, vol. 22, no. 8, pp. 881–884, 1995.

[22] A. W. Wernik, J. A. Secan, and E. J. Fremouw, "Ionospheric irregularities and scintillation," *Advances in Space Research*, vol. 31, no. 4, pp. 971–981, 2003.